RESEARCH PAPER

Impact of transition metal doping on the structural, optical and electrochemical performance of nanostructured lanthanum sesquioxide particles

S. Vishnu Priya [a], S. Gnanam [a*], J. Gajendiran [b]

[a] Department of Physics, School of Basic Sciences, Vels Institute of Science, Technology & Advanced Studies (VISTAS), Pallavaram, Chennai-600117, Tamil Nadu, India.

[b] Department of Physics & Centre for Materials Research, Vel Tech Rangarajan Dr. Sagunthala R&D Institute of Science and Technology, Avadi, Chennai 600062, Tamil Nadu, India.

*Corresponding author Email: gnanam.physics@gmail.com; gaja.nanotech@gmail.com

Abstract:

In this work, the microwave-precipitation process was successfully utilized to synthesize undoped lanthanum sesquioxide (ULSO) and Ni-doped lanthanum sesquioxide (NDLSO) nanostructured materials. Structural, optical and electrochemical properties of the synthesized ULSO and NDLSO samples were comprehensively characterized. Powder XRD analysis confirmed the formation of a hexagonal lanthanum sesquioxide (La_2O_3) crystal structure for all samples. Moreover, the crystallite size was gradually decreased with increasing Ni dopant concentration in comparison with the ULSO, which indicates that the Ni incorporation effectively reduced crystallite growth. The FTIR studies confirmed the existence of characteristic vibrational bands and functional groups of La_2O_3 in both ULSO and NDLSO samples. The optical absorption studies revealed an increase in the optical band gap with the increase of Ni concentration indicating the doping-induced modification of the electronic structure. Room-temperature PL emission (RTPLE) spectra exhibited intense blue–green emission arising from defect-related electronic states. Electrochemical investigations demonstrated that the NDLSO exhibited enhanced redox activity and improved charge-transfer behaviour compared with the ULSO, highlighting the beneficial influence of Ni doping on the multifunctional properties of La_2O_3 nanostructures.

Keywords: Rare-earth metal oxide; Transition metal dopant; Nanostructures; Structural analysis; Optical characteristics; Electrochemical properties

How to cite this article: S. Vishnu Priya a S. Gnanam a* J. Gajendiran b. Impact of transition metal doping on the structural, optical and electrochemical performance of nanostructured lanthanum sesquioxide particles. Int J Drug Deliv Technol. 2026;16(76s):2048-2054. DOI: 10.25258/ijddt.16.76s.197.

1. Introduction

Rare-earth sesquioxides (RESO) have attracted considerable research attention owing to their diverse functional properties, making them promising candidates for applications in material science, chemistry, physics, electronics and biomedicine. In the biomedical field, RESO have been extensively explored for drug delivery, bioimaging, tissue engineering, anticancer therapy, antimicrobial activity, and antioxidant applications [1-5]. Among these, lanthanum sesquioxide (La_2O_3) has emerged as an important RESO owing to its excellent physiochemical features, including a wide band gap (~5.5 eV), a high dielectric constant, superior thermal stability and favourable redox behaviour. These properties make La_2O_3 a suitable candidate for various applications such as catalysts, gas sensors, dielectric materials, optoelectronic devices, and energy storage systems [6,7]. One of the most effective approaches for tailoring the structural, optical, and electrical properties of RESO is cation doping. The electronic structure of the La_2O_3 lattice can be altered by doping the transition-metal (TM) ions [8]. Among the different TM dopants, nickel (Ni) doping has been widely investigated effectively due to its physicochemical features of La_2O_3 [9]. Ni incorporation causes lattice distortion, increases oxygen vacancy formation, and increases the density of electrochemically active surface sites, thus improving its optical, catalytic, and electrochemical performance [10,11]. Undoped and TM-doped La_2O_3 nanoparticles have been synthesized using a variety of physical and chemical methods, including sol-gel, hydrothermal, microwave-assisted synthesis, laser deposition, and co-precipitation techniques [12–14]. Among these methods, microwave-precipitation enables the preparation of highly homogeneous nanoparticles within a significantly shorter processing time compared with conventional synthesis routes.

In the current work, nanostructured RESO materials, such as undoped lanthanum sesquioxide (ULSO) and Ni-doped lanthanum sesquioxide (NDLSO) containing 1, 3, and 5 mol % Ni, were successfully synthesized via the microwave-precipitation route. The influence of Ni incorporation on the structural, optical, and electrochemical properties of La_2O_3 was systematically investigated and compared with those of ULSO. The synthesized ULSO and NDLSO samples were comprehensively characterized using powder X-ray diffraction (PXRD) studies to determine phase formation and crystallinity, Fourier transform infrared (FTIR) analysis to identify chemical bonding and functional groups, optical absorption studies to evaluate band gap, RTPLE analysis to study defect states and charge-carrier recombination, and CV analysis to investigate electrochemical performance.

2. Experimental procedure

At first, 0.1 M lanthanum trichloride heptahydrate and 0.3 M oxalic acid dihydrate were mixed in a molar ratio of 1:3 and dissolved in 100 ml of distilled water with continuous magnetic stirring for 45 min. White precipitate was formed as the resultant, indicating the precipitation of the lanthanum oxalate precursor. The resulting suspension was then subjected to microwave irradiation at 800 W for 10 min to promote rapid nucleation and crystal growth. Subsequently, the precipitate was separated by filtration, thoroughly washed with distilled water to remove residual impurities, and calcined in a muffle furnace at 450 °C for 2 h to obtain nanostructured La_2O_3. The same process was followed to synthesize Ni-doped La_2O_3 nanomaterials using 1%, 3% and 5 mol % nickel (II) acetate tetrahydrate as the Ni precursor, while maintain the other synthesis conditions constant.

Powder X-Ray Diffraction (PXRD) on a SmartLab SE X-RAY was used to investigate the crystallinity of the ULSO and NDLSO. The functional groups of the prepared ULSO and NDLSO were measured by Fourier Transform Infrared Spectroscopy (FT-IR, Perkin Elmer, Spectrum Two) in the spectral range of 400-4000 cm^{-1}. The optical properties like absorption and emission behaviour were studied by UV-Vis spectroscopy in the range of 200-800 nm (SHIMADZU, UV 3600 PLUS). The photoluminescence spectroscopy was characterized using JOBIN YVON FLUORIMETER in the range of 400-800 nm. The oxidation-reduction (redox) processes for the material were carried out through Cyclic Voltammetry (Versa STAT MC). Electrochemical measurements were evaluated using a three-electrode system with tetrabutylammonium perchlorate as the supporting electrolyte. A calomel electrode was employed as the reference electrode, while a platinum wire functioned as the counter electrode. The indicator electrode was fabricated by dispersing 1 mg of the 5% NDLSO sample in 20 mL of an aqueous solution and mixing the suspension uniformly.

3. Results and discussion:

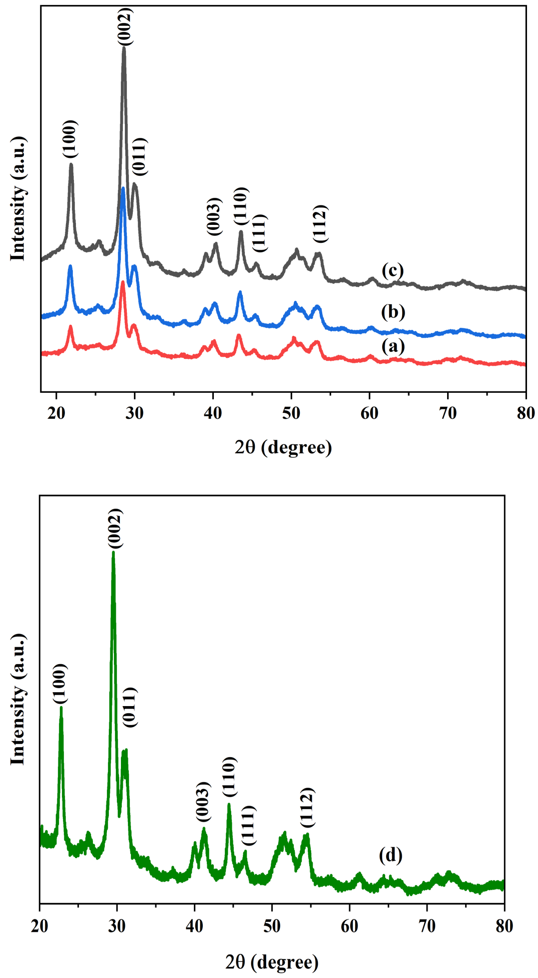

Fig. 1 PXRD plot of (a-c) 1%, 3% & 5% NDLSO and (d) ULSO samples.

Fig. 1(a-d) represents the PXRD patterns of 1%, 3% and 5% NDLSO and ULSO. The peak intensities which are observed as (100), (002), (011), (003), (110), (111) and (112) are indexed to the typical planes of the hexagonal lanthanum sesquioxide structure. The obtained reflections are highly matched with the standard JCPDS Card No. 73-2141 of ULSO in Fig. 1(d) [15]. After doping of Ni-ions, the diffraction profile of La_2O_3 remains stable with no other new peaks related to NiO or any other impurity phases, which displays the successful incorporation of Ni ions into the La_2O_3 matrix. The crystallite size of the synthesized ULSO and NDLSO samples was determined using the Debye-Scherrer's equation, which is displayed in the Table 1.

Table 1: Average crystallite size values of ULSO and NDLSO samples.

Samples	**2θ**	**FWHM**	**d-spacing**	**Average crystallite size, D= kλ/β cosθ (nm)**
ULSO	29.491	0.691	3.0264	11.89
1% NDLSO	29.0432	0.5196	3.0745	15.79
3% NDLSO	29.3027	0.6061	3.0479	13.54
5% NDLSO	29.0909	0.8659	2.9056	10.47

The FTIR spectra of 1%, 3% and 5% NDLSO and ULSO are depicted in the Fig. 2 (a-d). The wide band located at ~3440 cm^{-1} is due to the O-H stretching vibration of surface absorbed hydroxyl groups. The bands from ~1360 to 1500 cm^{-1} area are ascribed to the vibrations of carbonate groups, which are produced by the adsorption of CO_2 [16]. The prominent bands such as 513, 735 and 847 cm^{-1} are ascribed to the La-O lattice vibrations confirming the formation of La_2O_3.

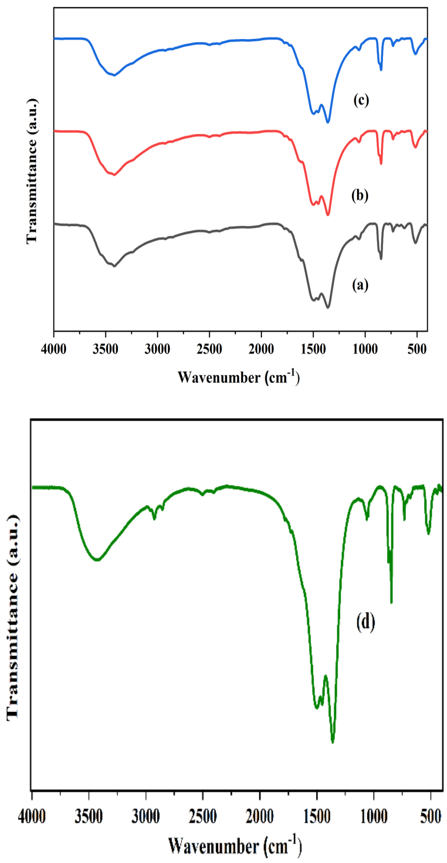

Fig. 2 FTIR plots of (a-c) 1%, 3% & 5% NDLSO and (d) ULSO.

The optical absorption spectra and Tauc plots of 1%, 3% and 5% NDLSO and ULSO samples are depicted in Fig. 3 & 4 (a-d). The UV region absorption is related to the intrinsic electronic transition of La_2O_3 related to the charge transfer from $O^{2-} \rightarrow La^{3+}$ (Fig. 3(d)) [17]. The strong absorption edge of pure La_2O_3 demonstrates its semiconductor properties. The doping of Ni ions causes the absorption edge to blue shift area due to the Ni-related defect levels in the La_2O_3 structure (Fig. 3 (a-c)) [18]. The increase in the band gap energy in the different ratios of NDLSO samples confirms the successful tuning of the electronic structure of the La_2O_3.

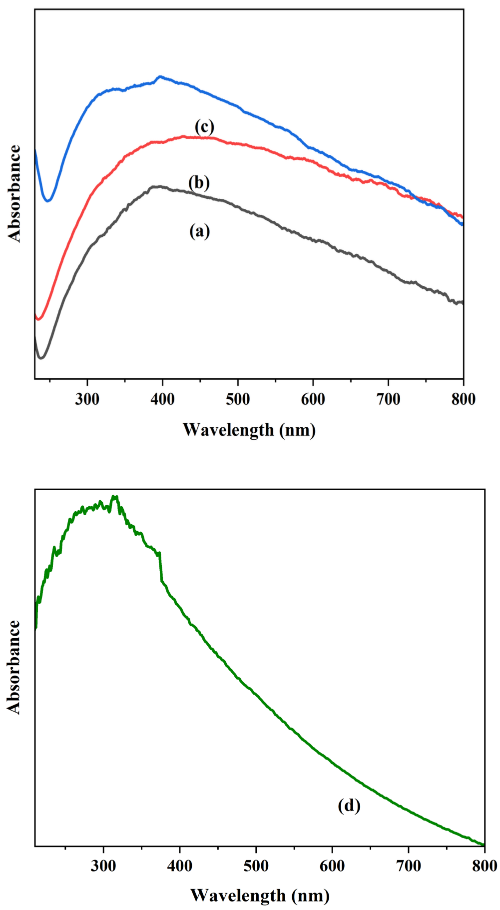

Fig. 3 Optical absorption spectra of (a-c) 1%, 3% & 5% NDLSO and (d) ULSO.

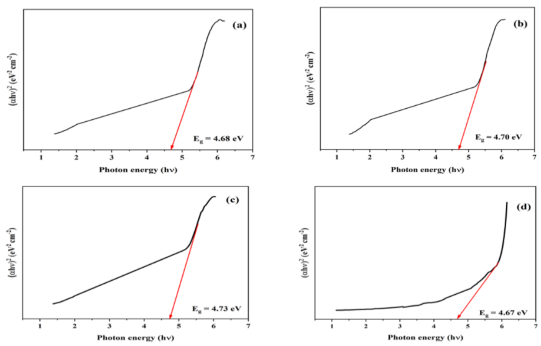

Fig. 4 Tauc plots of (a-d) 1%, 3% & 5% NDLSO and ULSO.

Fig. 5 (a-d) displays the RTPLE spectra of 1%, 3% and 5% NDLSO and ULSO samples, recorded using an excitation wavelength of 300 nm. A broad emission band centered at ~479-480 nm, corresponding to the blue to blue-green region of the visible spectrum, was observed. This emission is attributed to defect-assisted radiative recombination involving oxygen vacancies and surface defect states within the La_2O_3 lattice. Compared with ULSO, the PL emission intensity of NDLSO samples decreases progressively with increasing Ni concentration, indicating enhanced separation of photogenerated electron–hole pairs and suppressed radiative recombination. This behaviour suggests that Ni incorporation effectively tailors the electronic structure and defect levels of La_2O_3, in agreement with the defect evolution discussed in Fig. 5(a–c). In contrast, pure La_2O_3 displays a relatively strong and broad emission band with a maximum at 480 nm (Fig. 5(d)), which corresponds to blue-to-blue-green luminescence [19].

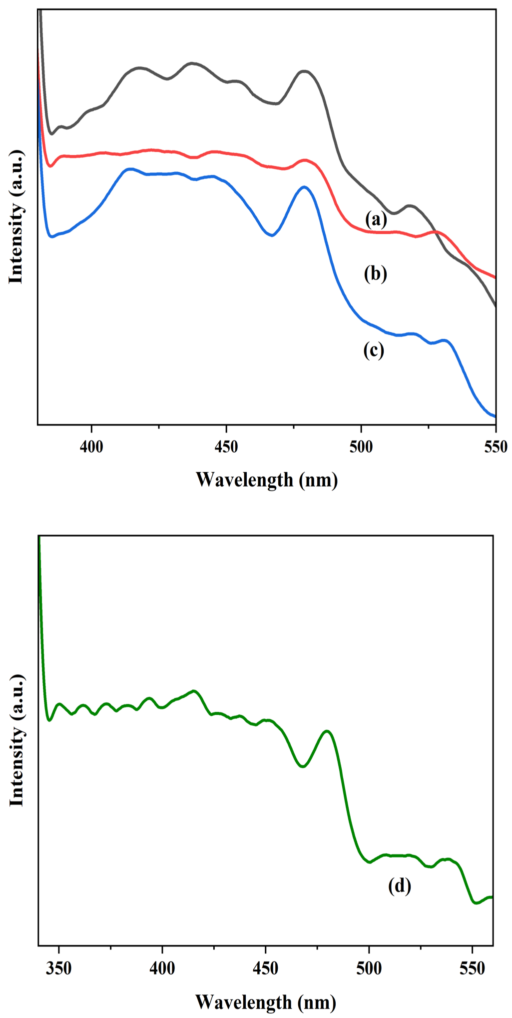

Fig. 5 RTPLE spectra of (a-c) 1%, 3% and 5% NDLSO and (d) ULSO samples.

The electrochemical behaviour of the synthesized 5% NDLSO sample at different scan rates from 10 to 100 mVs^{-1} shown in the Fig. 6(a). The increase of the current response with increasing scan rates reveals excellent electrochemical reversibility and enhanced charge transport capability. The specific capacitance decreases gradually with the increase of the scan rate, which can be attributed to the limited diffusion of electrolyte ions into the inner active sites of the electrode material (Fig. 6(b)). The electrical conductivity and capacitance properties are greatly enhanced by doping of Ni ions into La_2O_3. The Nyquist plot of the 5% NDLSO sample is presented in Fig. 6(c). The plot depicts a linear diffusion region at low frequencies, and the plot exhibits a semi-circular region at high frequencies corresponding to ion diffusion and charge-transfer resistance. The reduced semicircle diameter implies that the interfacial resistance is decreased and improved electron-transfer kinetics. In addition, the linear low-frequency region indicates efficient electrolyte ion diffusion and enhances charge-storage capability of the NDLSO electrode [20].

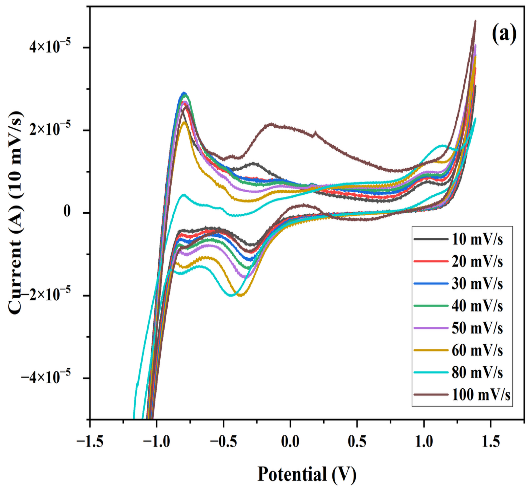

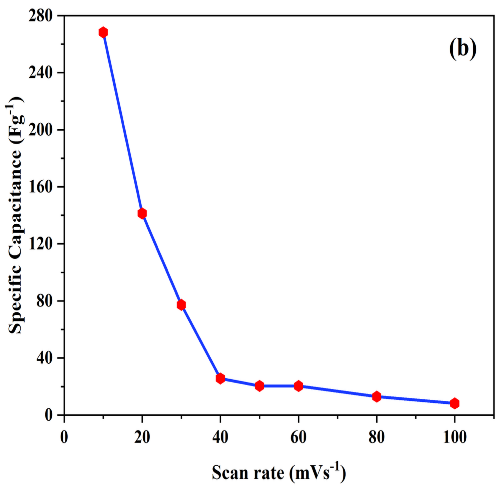

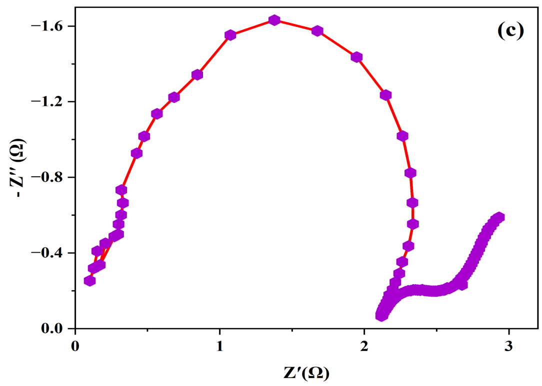

Fig. 6 (a) CV curve of 5% NDLSO at different scanning rates (b) Specific capacitance variation with respect to various scan rates (c) Nyquist curve of 5% NDLSO.

4. Conclusion

In this research work, nanostructured NDLSO and ULSO particles were successfully synthesized via microwave-precipitation technique. The PXRD analysis confirmed the hexagonal crystal structure of the synthesized NDLSO and ULSO samples whereas the molecular structural formation was further identified through FTIR studies. The optical properties of the nanostructured NDLSO and ULSO particles were studied by optical absorption and RTPLE spectra revealed their characteristic optical features. The synthesized NDLSO and ULSO samples band gap energies were found in the range of 4.67–4.73 eV. Furthermore, the RTPLE spectra exhibited the blue to blue-green emissions of the NDLSO and ULSO particles. The electrochemical performance of the nanostructured NDLSO sample was evaluated by determining its specific capacitance, which indicates its potential for energy storage applications.

References

[1] S. Pravitha, S. Priyanka, D. Devadathan, R. Raveendran, A review of functional rare earth metal oxides: Synthesis strategies, properties, and emerging applications, Coord. Chem. Rev. 558 (2026) 217767. https://doi.org/10.1016/j.ccr.2026.217767

[2] J.T.A. da Silva, L.A. Filgueiras, D.D. Araújo, A.J. Araújo, J.D.B. Marinho Filho, R.W.R. de Sousa, P.M.P. Ferreira, S.A. de Sousa, A.N. Mendes, Core–shell La_2O_3 nanoparticles functionalized with BSA: Synthesis, characterization, and selective cytotoxicity against fibroblasts, International Journal of Biological Macromolecules 336 (2026) 149217. https://doi.org/10.1016/j.ijbiomac.2025.149217

[3] P.S. Parab, A.A. Pawanoji, K.R. Jarhad, A.S. Pawar, Tailoring La_2O_3 nanomaterials through doping and coating for improved photocatalytic degradation, catalytic reduction, and other biological applications, Chemistry Select 10 (17) (2025) e202405740. https://doi.org/10.1002/slct.202405740

[4] R. Jbeli, M. Lahmar, C. Bilel, F. Saadallah, H.I. Ouzari, M. Bouaïcha, M. Amlouk, Structural and optical investigations on sprayed Co doped La_2O_3 thin films along with photocatalytic and anti-bacterial applications, Optik 242 (2021) 166837. https://doi.org/10.1016/j.ijleo.2021.166837

[5] S.A. Titova, M.P. Kruglova, V.A. Stupin, N.E. Manturova, E.V. Silina, Potential applications of rare earth metal nanoparticles in biomedicine, Pharmaceuticals 18 (2) (2025) 154. https://doi.org/10.3390/ph18020154

[6] Z.M. Riyas, S. Sharmila, P. Priya, M.R. Prabhu, Nanoengineering of hexagonal boron nitride (h-BN) decorated on La_2O_3 nanocomposite as an efficient electrode material for asymmetric supercapacitor application, Ionics 31 (2025) 4991–5011. https://doi.org/10.1007/s11581-025-06230-3

[7] S. Li, Y. Lin, Y. Wu, Y. Wu, X. Li, W. Tian, Ni doping significantly improves dielectric properties of La_2O_3 films, J. Alloys Compd. 822 (2020) 153469. https://doi.org/10.1016/j.jallcom.2019.153469

[8] L. Zhang, Z. Liu, Y. Chen, L. Zhang, X. Dai, S. Gao, J. Ren, A new high-efficiency nickel-based catalyst doped with rare earth metals for hydrogen production by ammonia decomposition, J. Indian Chem. Soc. 103 (2026) 102518. https://doi.org/10.1016/j.jics.2026.102518

[9] S. Berra, A. Mahroug, S. Hamrit, M.A. Azmin, A. Zoukel, S. Berri, N. Selmi, Experimental and DFT study of structural and optical properties of Ni-doped ZnO nanofiber thin films for optoelectronic applications, Opt. Mater. 134 (2022) 113188. https://doi.org/10.1016/j.optmat.2022.113188

[10] Z. Ma, Q. He, Z. Cui, Z. Yang, Y. Zou, C. Xiang, L. Sun, Nickel-doped lanthanum nitride catalysts for enhanced hydrogen storage in MgH_2: Synergistic kinetics improvement and reversible phase evolution mechanisms, J. Alloys Compd. 1036 (2025) 182078. https://doi.org/10.1016/j.jallcom.2025.182078

[11] A. Tiwari, P.P. Sahay, Modification in the physical properties of nanocrystalline ZnO thin films by M/Ni co-doping for transparent conductive oxide applications, Phys. B Condens. Matter 629 (2022), 413638, https://doi.org/10.1016/j.physb.2022.413638

[12] S.B. Jadhav, D.B. Malavekar, R.A. Mohite, S.B. Shaikh, K.V. Kadam, P.N. Pawaskar, J.H. Kim, N.-E. Lee, A critical review of lanthanum and lanthanum-based materials: Synthesis, applications, and challenges, Rare Met. 44 (2025) 5201–5232. https://doi.org/10.1007/s12598-024-03204-8

[13] P.E. Lokhande, S. Khasim, T.A. Hamdalla, D. Kumar, A. Vedpathak, U. Rednam, Exploring the synergistic potential of cerium and lanthanum oxides prepared via microwave-assisted sol–gel for energy storage applications, J. Sol-Gel Sci. Technol. 117 (2026) 57. https://doi.org/10.1007/s10971-025-07089-6

[14] A.K. Yadav, P. Singh, R. Pandey, Advances in lanthanum ferrite-based sensors: A comprehensive review, Anal. Sens. 5 (2025) e202400086. https://doi.org/10.1002/anse.202400086

[15] S. Karthikeyan, K. Dhanakodi, K. Shanmugasundaram, S. Surendhiran, Synthesis and characterization of lanthanum oxide nanoparticles: A study on the effects of surfactants, Mater. Today: Proc. 47 (2021) 901–906, https://doi.org/10.1016/j.matpr.2021.04.473

[16] S. Rahul, A. George, C.D. Savio, A. Dhayal Raj, S. Adarsh Rag, D. Daniel Lawrence, Unveiling radical trapping in La_2O_3 nanoparticles under hydrothermal temperature variations for enhanced photocatalysis, Mater. Chem. Phys. 358 (2026) 132415. https://doi.org/10.1016/j.matchemphys.2026.132415

[17] M. Mylarappa, C. Selvam, H.K. Sanjeevappa, S.G. Prasanna Kumar, G. Krishnamurthy, M.N. Kalasad, Reduced graphene oxide loaded La_2O_3 nanocomposite for dye degradation and antioxidant studies, Results Surf. Interfaces 14 (2024) 100202, https://doi.org/10.1016/j.rsurfi.2024.100202.

[18] Z. Yin, S. Li, X. Li, W. Shi, W. Liu, Z. Gao, M. Tao, C. Ma, Y. Liu, A review on the synthesis of metal oxide nanomaterials by microwave-induced solution combustion, RSC Adv. 13 (5) (2023) 3265–3277. https://doi.org/10.1039/D2RA07936D.

[19] G. Viswanathan, S. Ayyappan, B. Thirumalairaj, U. Krishnamoorthy, Tailoring photocatalytic performance: Lanthanum doping in nickel oxide for efficient degradation of some industrial cationic dyes in visible light radiation,

Desalination and Water Treatment 320 (2024) 100731. https://doi.org/10.1016/j.dwt.2024.100731
[20] D.A. Alshammari, M. Ikram, A. BaQais, S.U.K. Niazi, A. Irshad, M.A. Amin, M. Sohail, M.F. Warsi, Synthesis and supercapacitor application studies of aluminum-lanthanum co-doped bismuth oxide composite with N-doped reduced graphene oxide, Mater. Sci. Eng. B 310 (2024) 117720. https://doi.org/10.1016/j.mseb.2024.117720